ANL-ARC-188

# Report on Thermal Aging Effects on Tensile Properties of Ferritic-Martensitic Steels

**Nuclear Engineering Division**


ANL-ARC-188

# Report on Thermal Aging Effects on Tensile Properties of Ferritic-Martensitic Steels

**Meimei Li, W. K. Soppet, D. L. Rink, J. T. Listwan, and K. Natesan**
Nuclear Engineering Division
Argonne National Laboratory

June 2011

## ABSTRACT

This report provides an update on the evaluation of thermal-aging induced degradation of tensile properties of advanced ferritic-martensitic steels. The report is the first deliverable (level 3) in FY11 (M3A11AN04030103), under the Work Package A-11AN040301, "**Advanced Alloy Testing**" performed by Argonne National Laboratory, as part of Advanced Structural Materials Program for the Advanced Reactor Concepts. This work package supports the advanced structural materials development by providing tensile data on aged alloys and a mechanistic model, validated by experiments, with a predictive capability on long-term performance.

The scope of work is to evaluate the effect of thermal aging on the tensile properties of advanced alloys such as ferritic-martensitic steels, mod.9Cr-1Mo, NF616, and advanced austenitic stainless steel, HT-UPS. The aging experiments have been conducted over a temperature of 550-750°C for various time periods to simulate the microstructural changes in the alloys as a function of time at temperature. In addition, a mechanistic model based on thermodynamics and kinetics has been used to address the changes in microstructure of the alloys as a function of time and temperature, which is developed in the companion work package at ANL. The focus of this project is advanced alloy testing and understaning the effects of long-term thermal aging on the tensile properties.

Advanced materials examined in this project include ferritic-martensitic steels mod.9Cr-1Mo and NF616, and austenitic steel, HT-UPS. The report summarizes the tensile testing results of thermally-aged mod.9Cr-1Mo, NF616 H1 and NF616 H2 ferritic-martensitic steels. NF616 H1 and NF616 H2 experienced different thermal-mechanical treatments before thermal aging experiments. NF616 H1 was normalized and tempered, and NF616 H2 was normalized and tempered and cold-rolled. By examining these two heats, we evaluated the effects of thermal-mechanical treatments on material microstructures and associated mechanical properties during long-term aging at elevated temperatures.

Thermal aging experiments at different temperatures and periods of time have been completed: 550°C for up to 5000 h, 600°C for up to 7500 h, and 650°C for more than 10,000 h. Tensile properties were measured on thermally aged specimens and aging effect on tensile behavior was assessed. Effects of thermal aging on deformation and failure mechanisms were investigated by using in-situ straining technique with simultaneous synchrotron XRD measurements.

## TABLE OF CONTENTS

## LIST OF FIGURES

## LIST OF TABLES

# 1 Introduction

Advanced materials are a key element to the development of advanced nuclear energy systems. Advanced structural materials allow compact and simple design of reactor structure, and have the potential to reduce the construction and operational costs for next-generation nuclear reactors. Several advanced alloys have been selected for further development in support of sodium-cooled fast reactors (Busby et al 2008). R&D has focused on ferritic-martenstic steels, NF616 and NF616 with special thermal-mechanical treatment, and austenitic stainless steels, HT-UPS (High-Temperature Ultrafine Precipitate-Strengthened) steel.

NF616 is a variant of mod.9Cr-1Mo (G91) ferritic-martensitic steel, the alloy developed in 1980s for applications in liquid metal fast breeder reactors. NF616 and mod.9Cr-1Mo have improved high temperature strength and creep properties compared to Sandvik HT-9, a ferritic-martensitic steel traditionally considered for liquid metal fast reactors (Klueh and Harries 2001). NF616 offers the best high temperature strength among commercially available ferritic steels. The high temperature strength and creep resistance of NF616 and mod.9Cr-1Mo rely on tempered martensitic microstructure stabilized by $M_{23}C_6$ carbides, a fine distribution of vanadium/niobium carbon-nitride (MX) precipitates, and solution strengthening by Mo (and W) (Klueh and Harries 2001).

The HT-UPS, a 14Cr-16Ni austenitic stainless steel containing nanometer-sized Ti+Nb+V carbide precipitates, possesses increased creep resistance and irradiation tolerance over traditional 316 SS. Because advanced materials heavily rely on second-phase fine precipitate particles for improved high temperature strength, creation and maintenance of the precise microstructure during fabrication and heat treatment and during service is the key to obtain their superior properties. The properties of advanced materials generally degrade with time, when exposed to high temperatures. Significant microstructural changes during prolonged thermal exposure can lead to dramatically different responses to service environments. Research has shown that long-term exposure of NF616 and mod.9Cr-1Mo to high temperatures can result in significant microstructural changes, leading to degradation at high temperature performance and as well as embrittlement at low temperatures (Klueh and Harries 2001). Microstructural stability and mechanical property degradation over long-term aging is also a major concern for the nuclear structural applications of these advanced alloys. It is critically important to understand the fundamental relationship between microstructures and mechanical behavior such that aging-induced degradation of mechanical performance and failure can be reliably predicted in materials and components.

The objective of this project is to evaluate the effect of thermal aging on the tensile properties of advanced alloys such as ferritic-martensitic steels, mod.9Cr-1Mo, NF616, and advanced austenitic stainless steel, HT-UPS. The aging experiments have been conducted over a temperature range of 550-750°C for various time periods to simulate the microstructural changes in the alloys as a function of time at temperature. The companion project is being conducted at ANL to develop a mechanistic model based on thermodynamics and kinetics to address the changes in microstructure of the alloys as a function of time and temperature. The focus of this project is advanced alloy testing and understanding the effects of long-term thermal aging on the tensile properties.

## 2 Materials

Three classes of alloys were investigated, including ferritic-martensitic steels, NF616, G91, and advanced austenitic stainless steel, HT-UPS. G91 steel was used as a reference to compare with NF616. G91 steel was in plate form with a thickness of 0.375". It was normalized at 1050°C and tempered at 760°C for 1 h and air cooled. Two heats of NF616 were studied. Heat 1 of NF616 (referred to H1 NF616) was in 1"-thick plate form, normalized at 1050°C and tempered at 750°C for 2 h and air cooled. Heat 2 of NF616 (referred to H2 NF616) was 0.030" thick sheet. The processing of H2 NF616 involved hot rolling of a 0.325" thick plate to 0.110" thick sheet, air cooling, a subsequent heat treatment at 1080°C for 0.5 h and tempering at 750°C for 2 h, air cooling, and a final cold-rolling to a 0.030" thick sheet.

Two heats of HT-UPS were examined. Heat AX-6 was in sheet form with a thickness of 2 mm. It was annealed at 1200°C for 1 h (referred to SA HT-UPS). The second heat of HT-UPS was in plate form with a thickness of 0.75". The final process was hot rolling at 1200°C followed by air cooling (referred to HR HT-UPS). All five materials were provided by Oak Ridge National Laboratory (ORNL). The chemical compositions of H2 NF616 and HR HT-UPS were provided by ORNL. The chemical analysis for G91, H1 NF616, and SA HT-UPS was carried out by Bodycote Materials Testing. The chemical compositions are given in Table 1. The heat treatment conditions are summarized in Table 2.

The microstructure of the alloys was characterized by optical microscopy, scanning electron microscopy, transmission electron microscopy, and high-resolution synchrotron x-ray diffraction. Optical micrographs showing the as-received microstructure for H1 NF616, H2 NF616, G91, SA HT-UPS, and HR HT-UPS steels are given in Fig. 1.

## 3 Thermal Aging Experiments and Tensile Tests

Thermal aging experiments were performed at temperatures between 550 and 750°C for various exposure times to examine microstructural evolution during long-term thermal aging and its effects on tensile properties. Two types of sheet-type tensile specimens were used in the thermal aging experiments and follow-up tensile tests, one type with a short grip section, and another with an extended grip section, which are schematically shown in Fig. 2. The extended grip portion of the specimen was used for microstructural characterization of the same specimen to be used for tensile property measurements. The tensile specimens were electrical-discharge-machined with the gage parallel to the rolling direction. The tensile specimens have gage dimensions of $7.62 \times 1.52 \times 0.75$ mm.

Each tensile specimen was wrapped in Ta foil, and encapsulated in a vacuum quartz tube, as shown in Fig. 3(a). Encapsulated specimens were loaded in an air furnace heated to the target temperature for an extended period [Fig. 3(b)].

Thermally aged specimens were tested under uniaxial tension to examine the effects of thermal aging on tensile properties. Tensile tests were performed on a MTS screw-driven machine at room temperature or the aging temperature in air at a nominal strain rate, 0.001 $s^{-1}$. A

tensile specimen was heated in a three-zone air furnace. The applied load was recorded by a load cell and the specimen displacement was recorded using a linear variable differential transformer (LVDT) attached to the load train. The engineering tensile properties were determined from an analysis of the load vs. displacement data files. Fig. 4 shows the set-up of high temperature tensile testing.

Microhardness measurements were performed on the grip end of some tensile specimens. Three to five measurements were made on each specimen, and the average values of hardness are reported.

In-situ straining technique with simultaneous synchrotron x-ray diffraction (XRD) and scattering measurements provides a state-of-the-art capability to examine concurrent microstructural evolution and associated deformation and failure mechanisms in bulk materials, ideal for developing a microstructure-based deformation and fracture understanding and predictive model. To explore the use of this advanced in-situ synchrotron radiation technique, we have performed in situ XRD experiment on as-received G91 steel under thermal-mechanical loading at the APS, and obtained valuable information on crystallographic orientation and phase-dependent stress-strain behavior.

In situ high-energy synchrotron x-ray experiments were carried out during tensile loading at room temperature and at 550°C. A sheet-type tensile specimen was used for continuous measurements by x-ray diffraction during tensile loading until failure. A thermocouple was spot-welded in the gauge section of the tensile specimen to monitor specimen temperature. Load and displacement data were recorded and used to determine the macroscopic stress-strain curve and tensile properties. Diffraction measurements were conducted with a monochromatic 115 keV (k = 0.10798 Å) and 86 keV (k = 0.14416 Å) x-ray beam in transmission with a beam size of 300 × 300 $\mu m^2$. Debye-Scherrer diffraction rings were recorded using an area detector. A schematic layout of the in-situ straining and synchrotron radiation measurements is given in Fig. 5. Lattice strains were calculated from changes in the measured lattice spacing relative to the lattice spacing prior to tensile deformation. The measured lattice strains represent an average value of the strain in a direction perpendicular to the particular set of crystallographic planes giving the reflection.

Table 1. Chemical composition (in wt%) of the selected alloys

| Alloy | Fe | C | Mn | P | S | Si | Ni | Cr | Mo | B | Ti | Nb | V | N | W |
|---|---|---|---|---|---|---|---|---|---|---|---|---|---|---|---|
| SA HT-UPS | Bal | 0.06 | 2.13 | 0.038 | 0.009 | 0.10 | 16.86 | 14.63 | 2.66 | 0.0044 | 0.29 | 0.11 | 0.53 | - | - |
| HR HT-UPS | Bal | 0.058 | 2.08 | 0.048 | 6 ppm | 0.28 | 16.06 | 14.54 | 2.33 | 0.007 | 0.15 | 0.15 | 0.53 | 0.028 | |
| H1 NF616 | Bal | 0.11 | 0.46 | 0.009 | <0.005 | 0.03 | 0.06 | 9.09 | 0.43 | 0.0009 | - | 0.08 | 0.20 | 0.057 | 1.84 |
| H2 NF616 | Bal | 0.092 | 0.45 | 0.007 | 0.011 | 0.15 | 0.21 | 9.02 | 0.45 | 0.0023 | | 0.07 | | 0.03 | 1.71 |
| G91 | bal | 0.09 | 0.46 | 0.012 | <0.005 | 0.41 | 0.11 | 8.33 | 1.04 | 0.05 | - | 0.05 | 0.22 | 0.059 | - |

Table 2. Heat treatment conditions

| Alloy | Heat treatment |
|---|---|
| SA HT-UPS | Annealed at 1200°C for 1 h |
| HR HT-UPS | Hot-rolled at 1200°C |
| H1 NF616 | Normalized at ~1050°C and tempered at 750°C for 2 h and air cooled |
| H2 NF616 | Normalized at 1080°C for 0.5 h and tempered at 750°C for 2 h, air cooling, and cold-rolled |
| G91 | Normalized at 1050°C and tempered at 760°C for 1 h and air cooled |

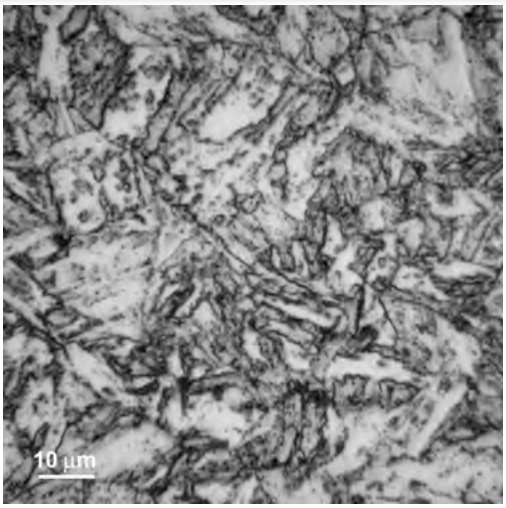


H1 NF616

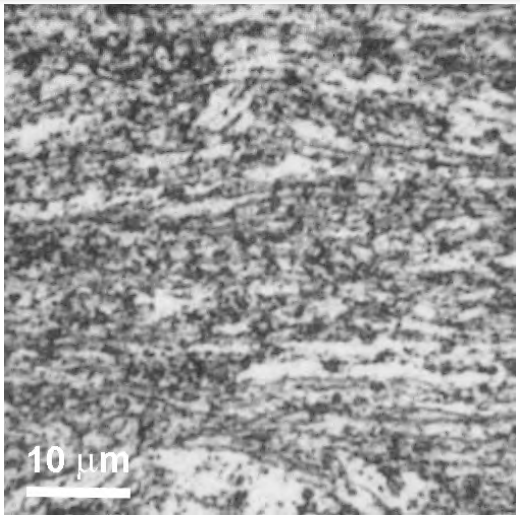


H2 NF616

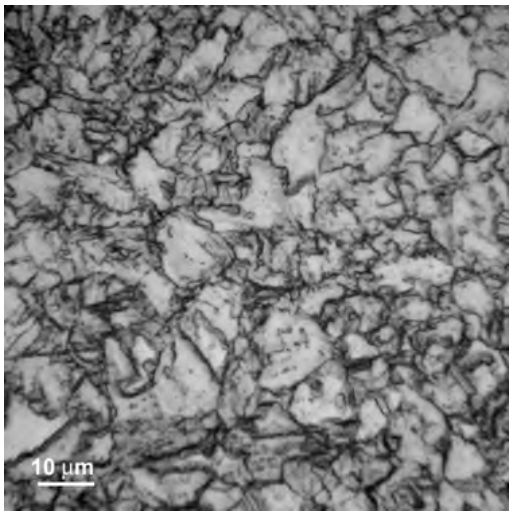


G91

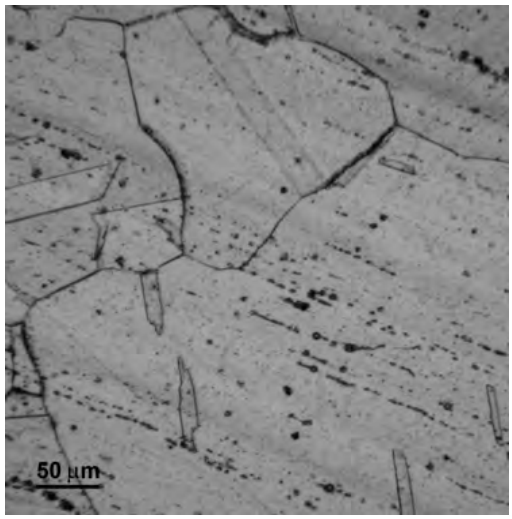


SA HT-UPS

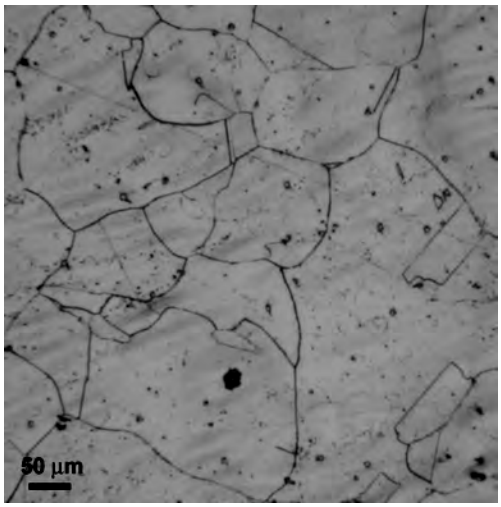


HR HT-UPS

Figure 1. Optical micrographs showing the microstructure of as-received H1 NF616, H2 NF616, G91, SA HT-UPS, and HR HT-UPS steels.

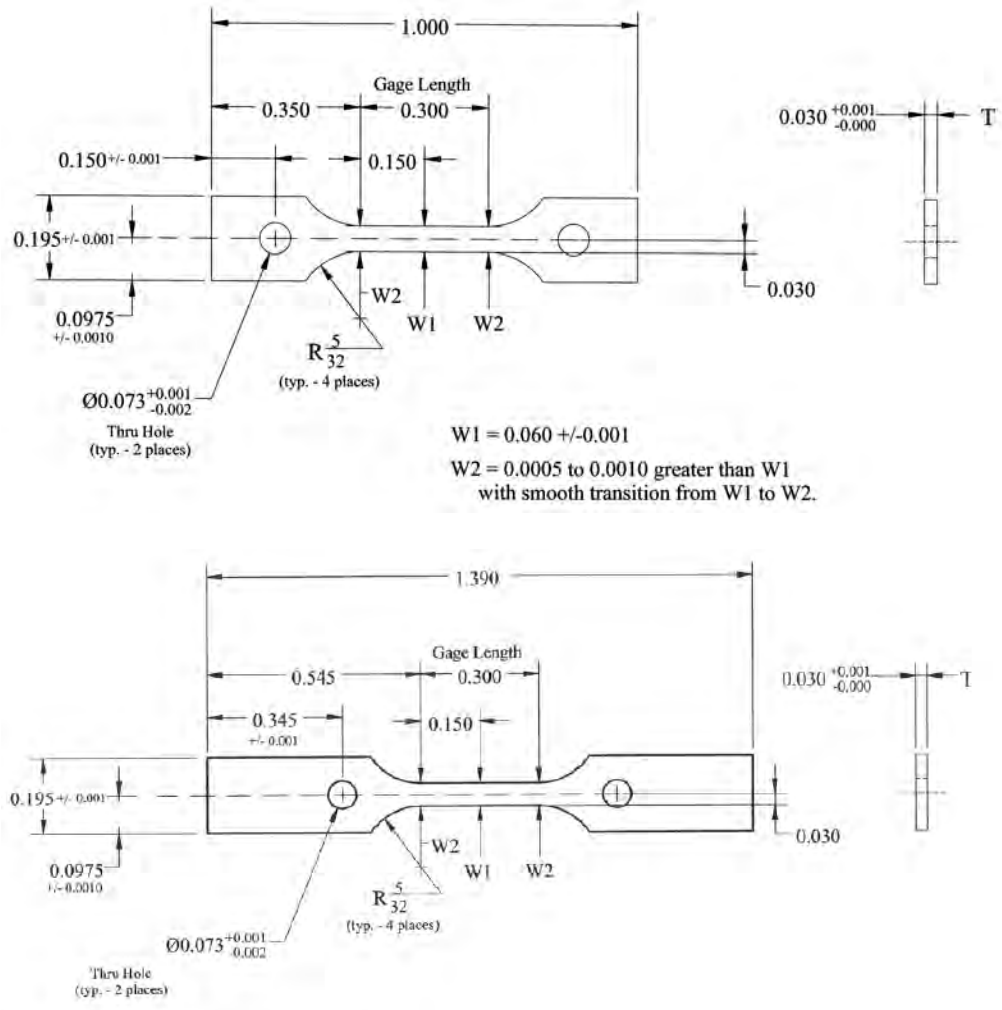


Figure 2. Schematic drawing of sheet-type tensile specimens (unit: inch).

(a) (b)

Figure 3. (a) A tensile specimen wrapped in Ta foil and encapsulated in vacuum and (b) capsules loaded in an air furnace for thermal aging.

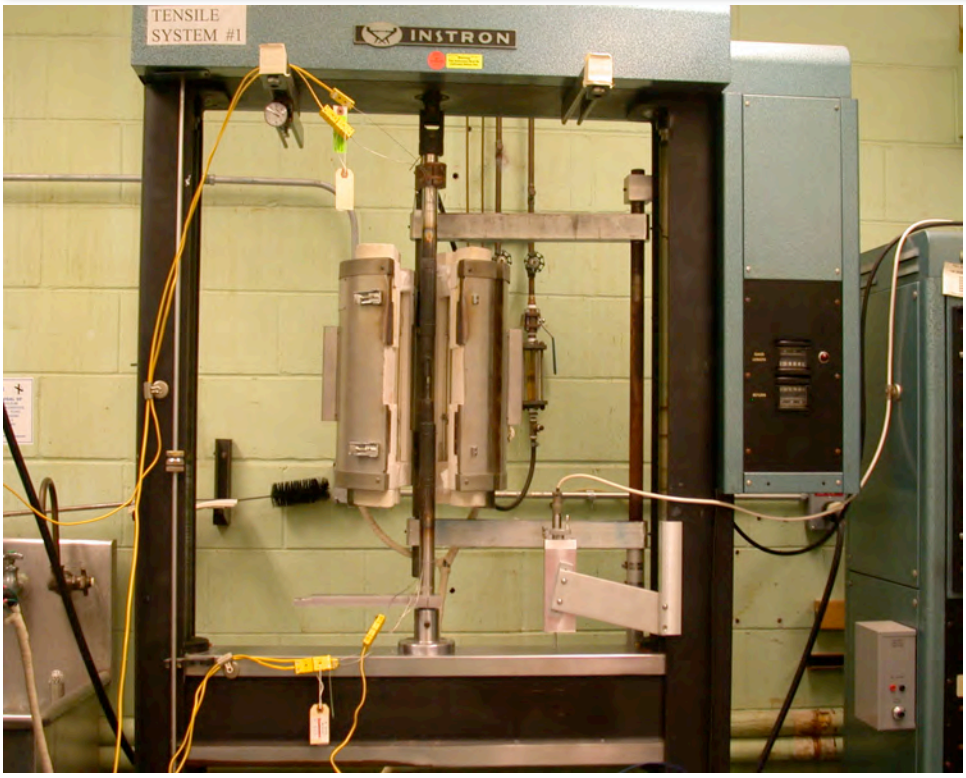


Figure 4. Experimental set-up of high temperature tensile testing.

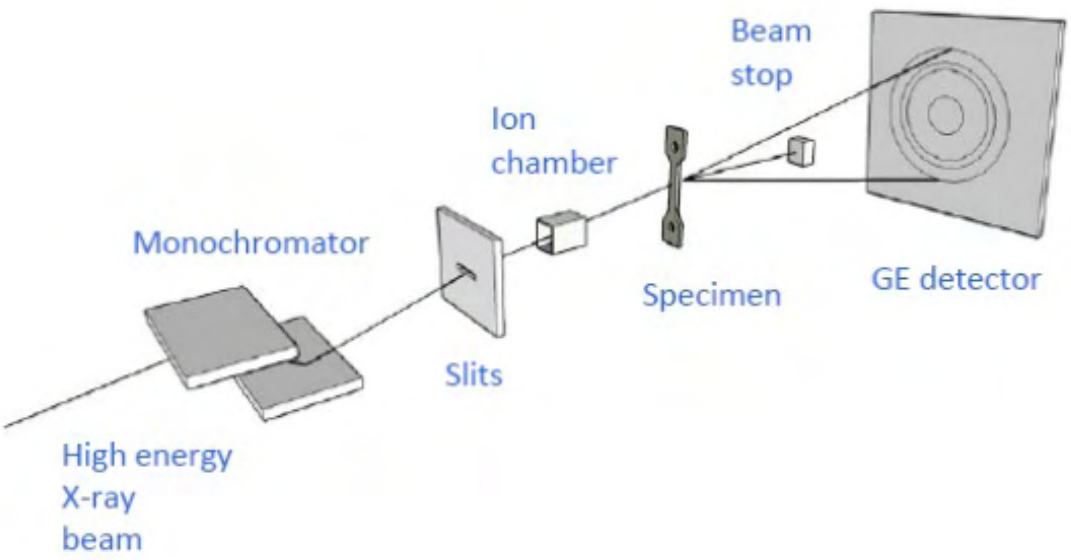


Figure 5. Experimental setup for *in situ* straining and synchrotron XRD measurements at the APS.

# 4 Results of Tensile Tests

## *4.1 Stress-Strain Curves*

The engineering stress-strain curves of as-received and thermally-aged specimens for mod.9Cr-1Mo steel are given in Figs. 6-9. Figure 6 shows the stress-strain curves for normalized and tempered (as-received) mod.9Cr-1Mo tested at temperatures between 20 and 650°C. Note that the material strength decreased and the ductility increased significantly with increasing test temperature. The most important feature is that the material lost nearly all the strain hardening capability even at 550°C with the uniform elongation less than 2%.

Figure 7 shows the stress-strain curves of mod.9Cr-1Mo steel thermally-aged for up to 5000 h at 550°C. Note that the specimen exposed to liquid sodium at 550°C for 2700 h is included in Fig. 7. The microstructural characterization of the sodium-exposed specimen showed nearly no effects of sodium corrosion under this temperature and exposure time. The changes in tensile properties are believed to be primarily due to the thermal effect, though theoretical calculations and experimental characterizations are needed to confirm that no significant decarburization/carburization occurred in these specimens. As shown in Fig. 7, the thermal exposure at 550°C for up to 5000 h had minimal effect on the alloy strength and slight increase in ductility.

Figure 8 shows the stress-strain curves of mod.9Cr-1Mo steel thermally aged for up to 7500 h at 600°C. A reduction in material strength is evident under such thermal aging condition. Figure 8 shows the stress-strain curves of mod.9Cr-1Mo steel thermally aged for up to 10650 h at 650°C. Salient features include strength reduction and ductility loss after extended exposure at 650°C.

The engineering stress-strain curves of as-received and thermally aged specimens for NF616 H1 are given in Figs. 10-13. Figure 10 shows the stress-strain curves for normalized and tempered (as-received) NF616 H1 steel tested at temperatures between 20 and 650°C. Similar to the tensile response of normalized and tempered mod.9Cr-1Mo steel, the material strength decreased and ductility increased significantly with increasing test temperature. Again, the alloy lost nearly all the strain hardening capability even at 550°C, with uniform elongation less than 2%. Figure 11 shows the stress-strain curves of NF616 H1 steel thermally aged for up to 5000 h at 550°C. Figure 11 also includes data for the specimen exposed to liquid sodium at 550°C for 2700 h. The thermal exposure at 550°C for up to 5000 h had minimal effect on the alloy strength and slight improvement in ductility.

Figure 12 shows the stress-strain curves of NF616 H1 steel thermally aged for up to 7500 h at 600°C. A reduction in material strength is evident under such thermal aging condition. What distinguishes NF616 H1 from mod.9Cr-1Mo is its significant ductility loss after thermal exposure for 7500 h at 600°C. Figure 13 shows the stress-strain curves of NF616 H1 steel thermally aged for up to 10650 h at 650°C. Strength reduction is pronounced after thermal exposure for 10650 h. The material ductility reduced initially and then recovered as exposure time increased.

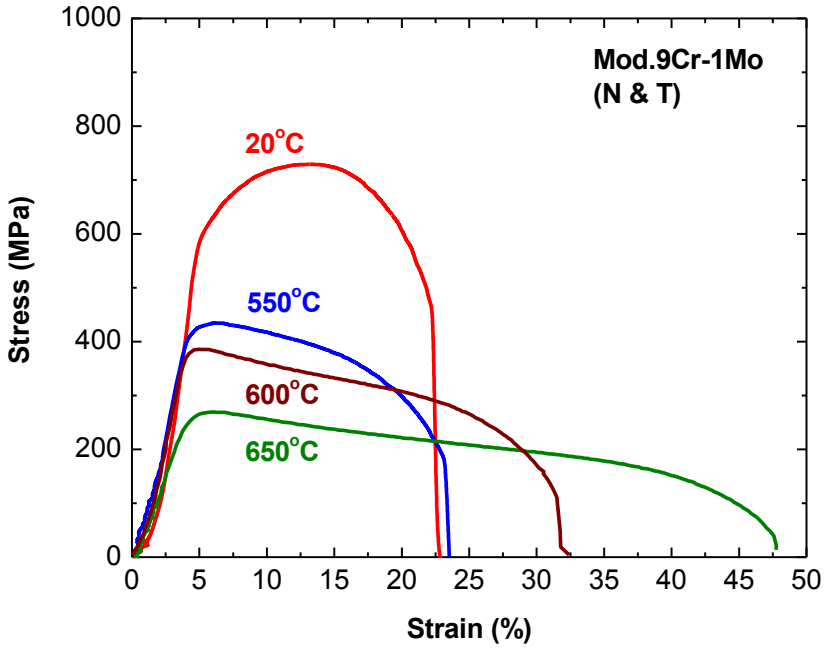


Figure 6. Stress-strain curves of normalized and tempered mod.9Cr-1Mo steel tested at temperatures between 20 and 650°C.

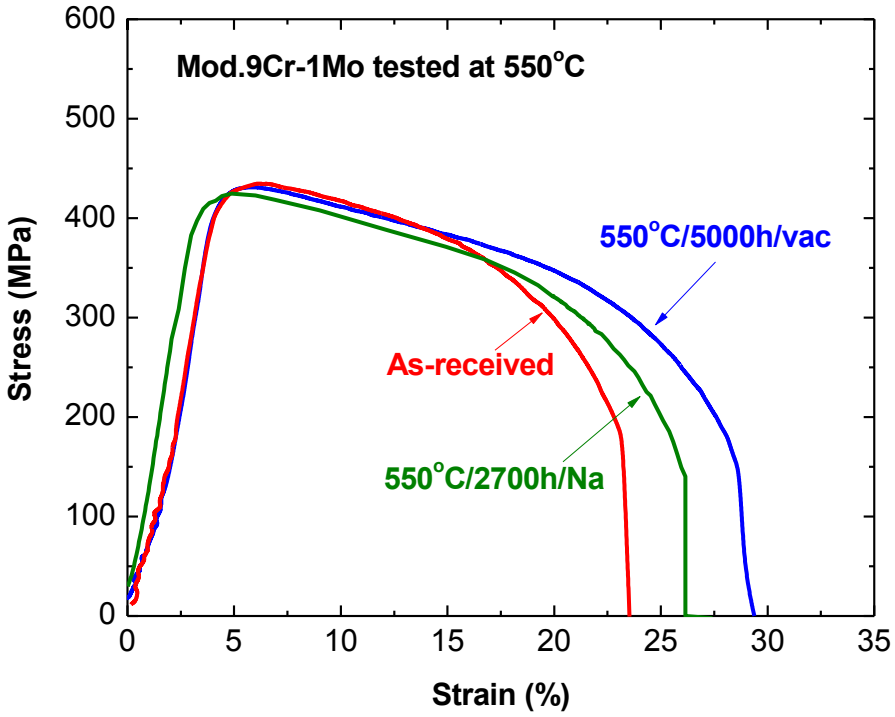


Figure 7. Stress-strain curves of mod.9Cr-1Mo steel thermally aged at 550°C for up to 5000 h and tested at 550°C.

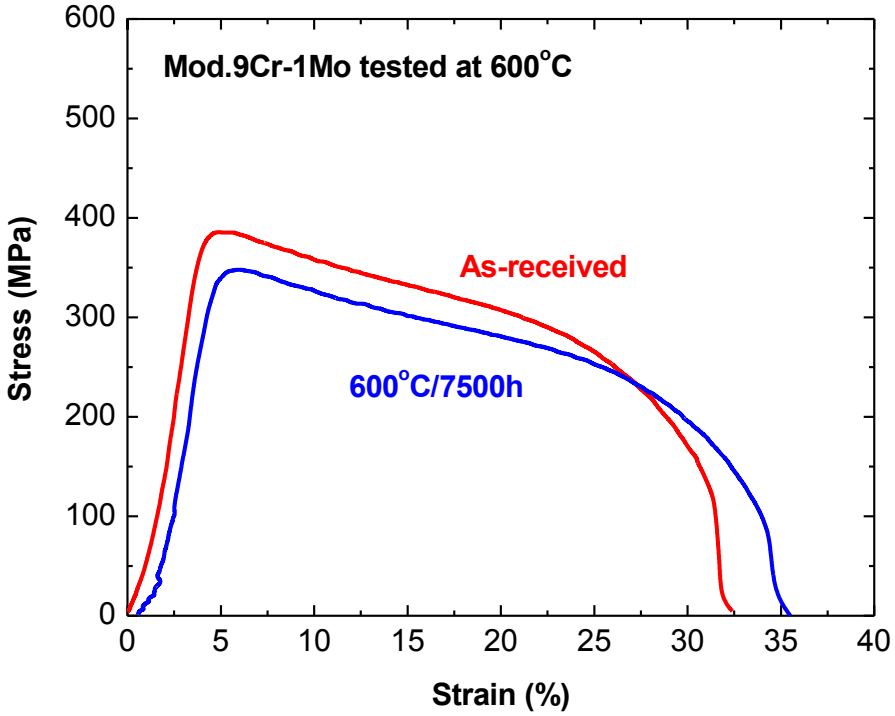


Figure 8. Stress-strain curves of mod.9Cr-1Mo steel thermally aged at 600°C for up to 7500 h and tested at 600°C.

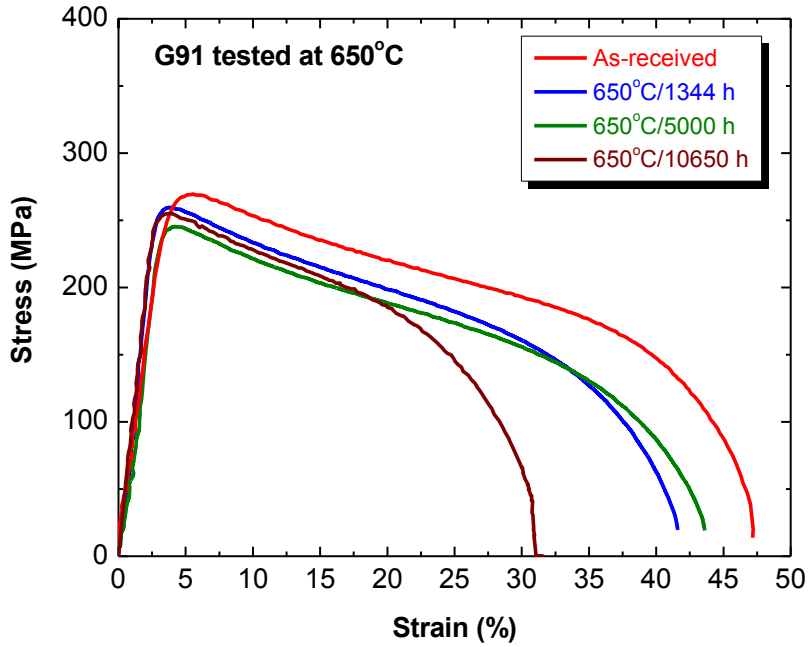


Figure 9. Stress-strain curves of mod.9Cr-1Mo steel thermally aged at 650°C for up to 10650 h and tested at 650°C.

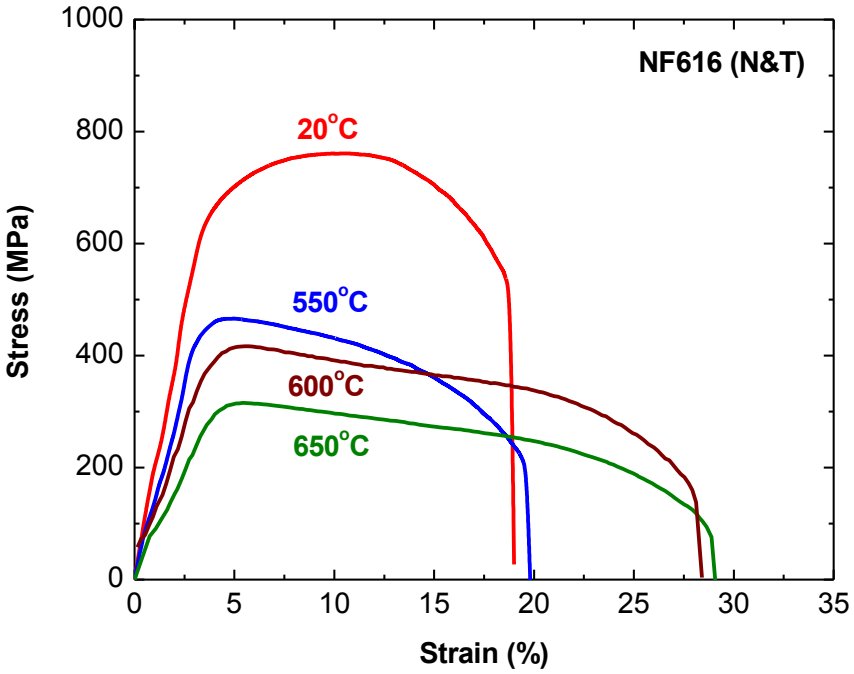


Figure 10. Stress-strain curves of normalized and tempered NF616 (H1) steel tested at temperatures between 20 and 650°C.

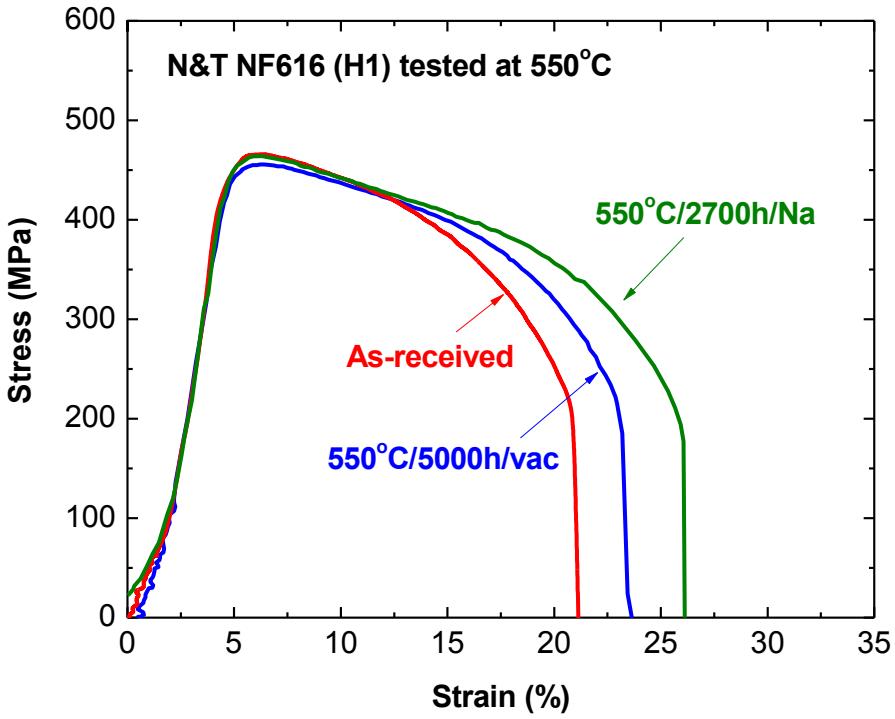


Figure 11. Stress-strain curves of normalized and tempered NF616 (H1) steel thermally aged at 550°C for up to 5000 h and tested at 550°C.

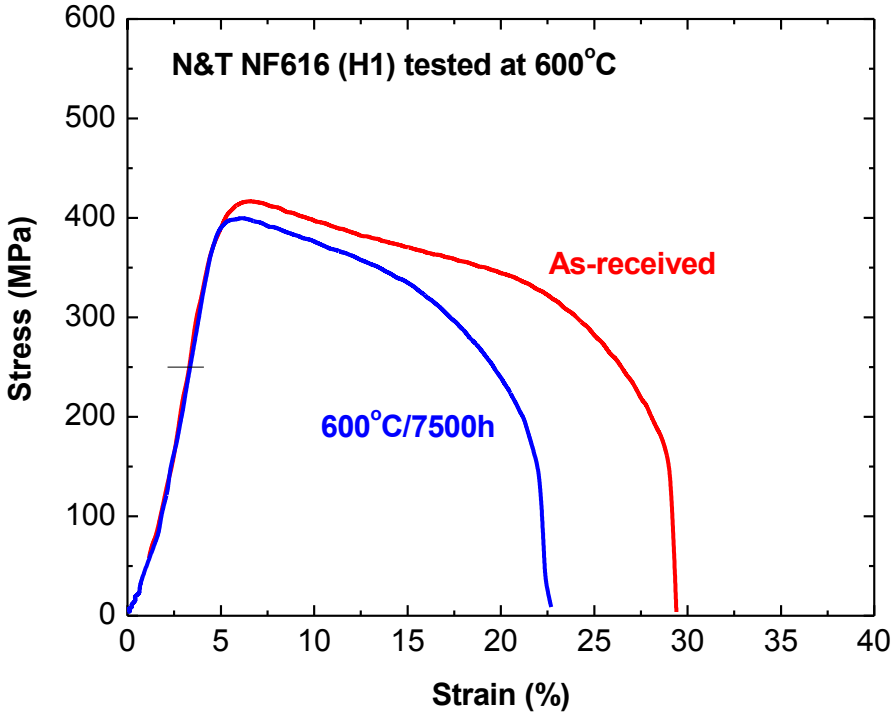


Figure 12. Stress-strain curves of normalized and tempered NF616 (H1) steel thermally aged at 600°C for up to 7500 h and tested at 600°C.

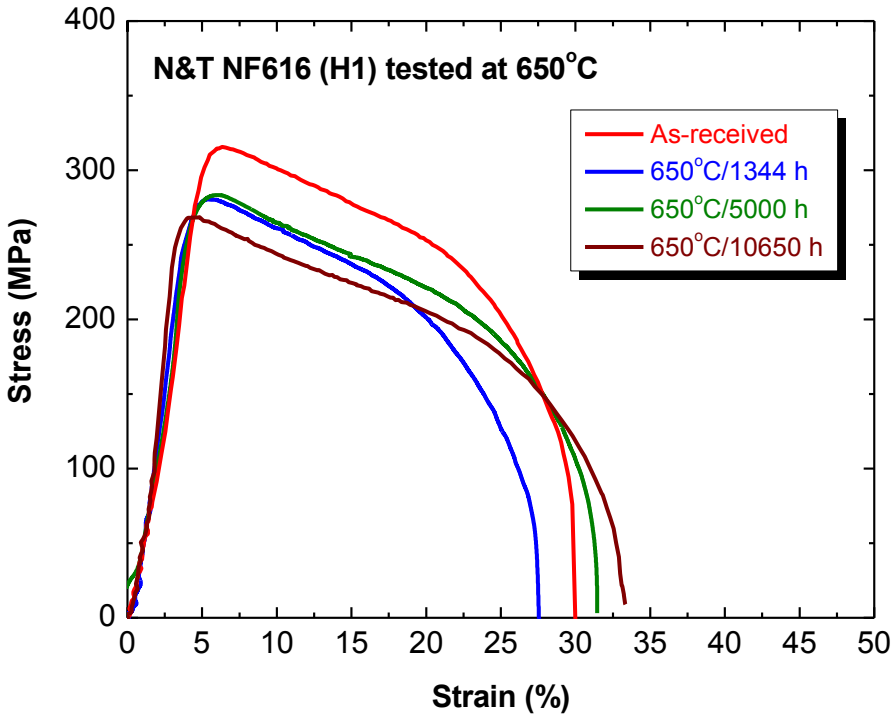


Figure 13. Stress-strain curves of normalized and tempered NF616 (H1) steel thermally aged at 650°C for up to 10650 h and tested at 650°C.

The engineering stress-strain curves of as-received and thermally-aged specimens for NF616 H2 are given in Figs. 14-16. Note that NF616 H2 was cold-rolled after initial normalized and tempered treatment. It is important to understand how the different thermal-mechanical treatment affects material's tensile behavior of high-strength ferritic-martensitic steels. Figure 14 shows the stress-strain curves for as-received NF616 H2 steel tested at temperatures between 550 and 650°C. Similar to the tensile response of normalized and tempered mod.9Cr-1Mo steel and NF616 H1, the alloy lost nearly all the strain hardening capability even at 550°C with the uniform elongation less than 2%. Note that in the temperature range of 550-650°C, the material strength decreased and the ductility increased significantly with increasing test temperature.

Figure 15 shows the stress-strain curves of NF616 H2 steel thermally aged for 2700 h in sodium at 550°C. The exposure had nearly no effect on the alloy strength and reduced its ductility.

Figure 16 shows the stress-strain curves of NF616 H2 steel thermally aged for 1200 h at 650°C. Even with such short term exposure at 650°C, the alloy strength was reduced drastically. It is also interesting to note that the alloy gains some strain hardening capability after exposure.

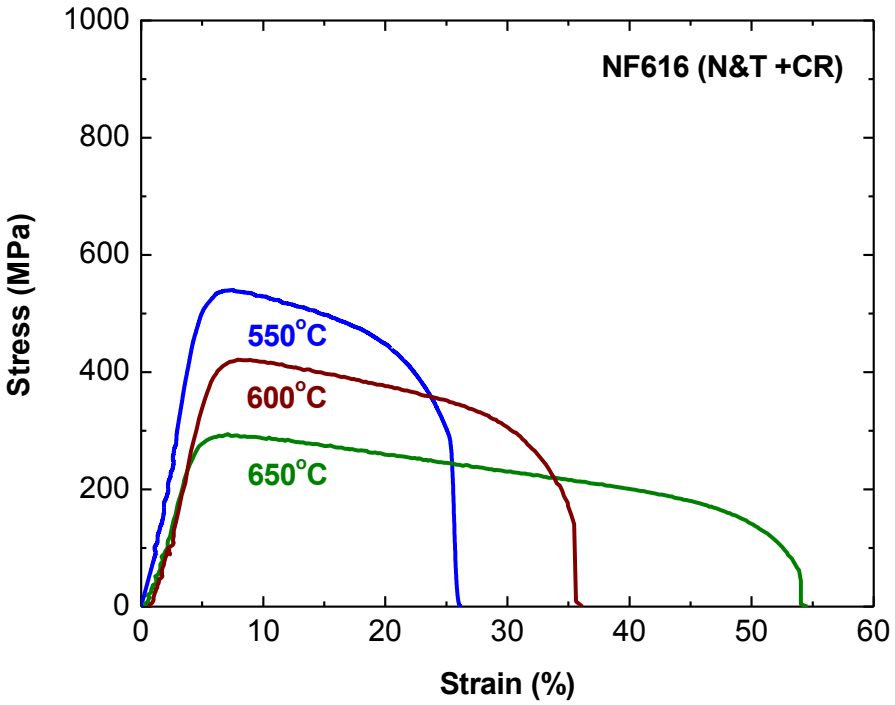


Figure 14. Stress-strain curves of normalized and tempered and cold-rolled NF616 (H2) steel tested at temperatures between 20 and 650°C.

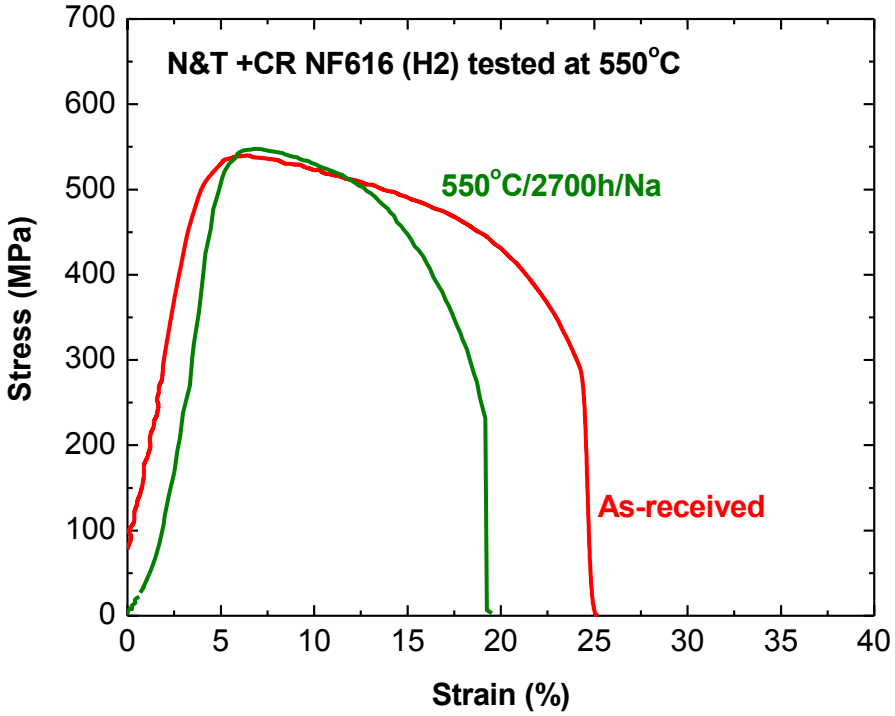


Figure 15. Stress-strain curves of normalized and tempered and cold-rolled NF616 (H2) steel thermally-aged at 550°C for up to 2700 h and tested at 550°C.

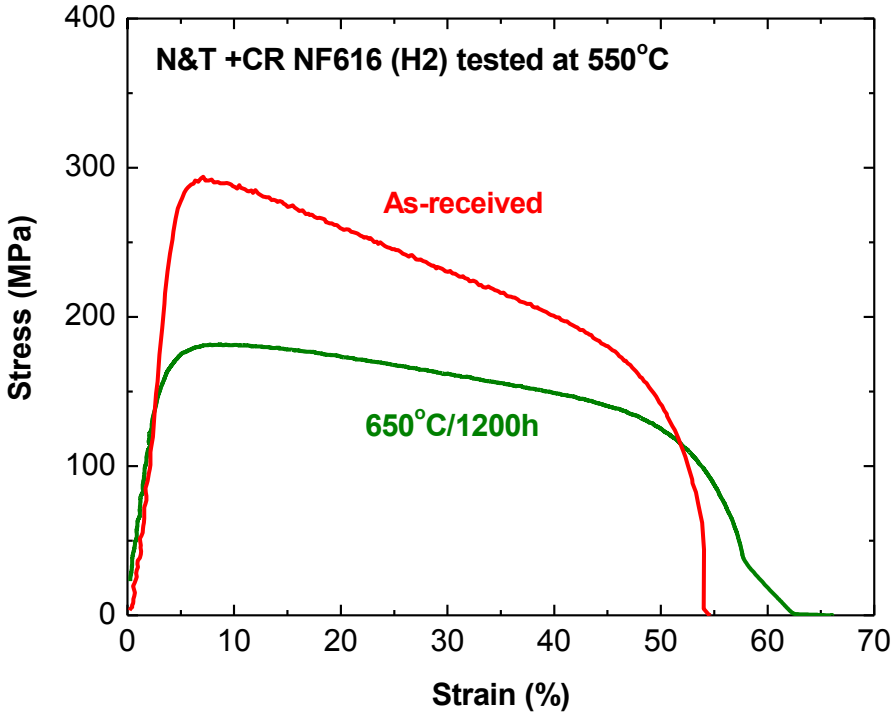


Figure 16. Stress-strain curves of normalized and tempered and cold-rolled NF616 (H2) steel thermally aged at 650°C for up to 1200 h and tested at 650°C.

### *4.2 Effects of Thermal Aging on Tensile Properties*

A summary of tensile properties, yield stress (YS), ultimate tensile strength (UTS), uniform elongation (UE) and total elongation (TE), and hardness, of thermally aged specimens for mod.9Cr-1Mo, NF616 H1 and NF616 H2 steels is given in Table 3. The effects of thermal aging on tensile properties are shown in Figs. 17-19 for aging temperatures of 550, 600, and 650°C, respectively. Thermal aging at 550°C for up to 5000 h has insignificant effect on the YS and UTS of these three materials. The NF616 H2 (cold-rolled) showed reduction in total elongation even after exposure for 2700 h. The thermal aging data at 600°C are available only for mod.9Cr-1Mo and NF616 H1. Comparing these two alloys, the thermal exposure for 7500 h had minimal effect on the strength of NF616 H1 and decreased the strength of mod.9Cr-1Mo. The ductility of mod.9Cr-1Mo increased and the ductility of NF616 H1 decreased after the thermal exposure. Thermal exposure at 650°C reduced the UTS of all three alloys. The effect is strongest in NF616 H2. Even after 1200 h exposure at 650°C, both the YS and UTS of NF616 H2 was reduced 40-50%. What is interesting is NF616 H2 regained some strain hardening capability after thermal exposure at 650°C, while neither mod.9Cr-1Mo nor NF616 H1 showed such behavior, even after exposure for >10,000 h.

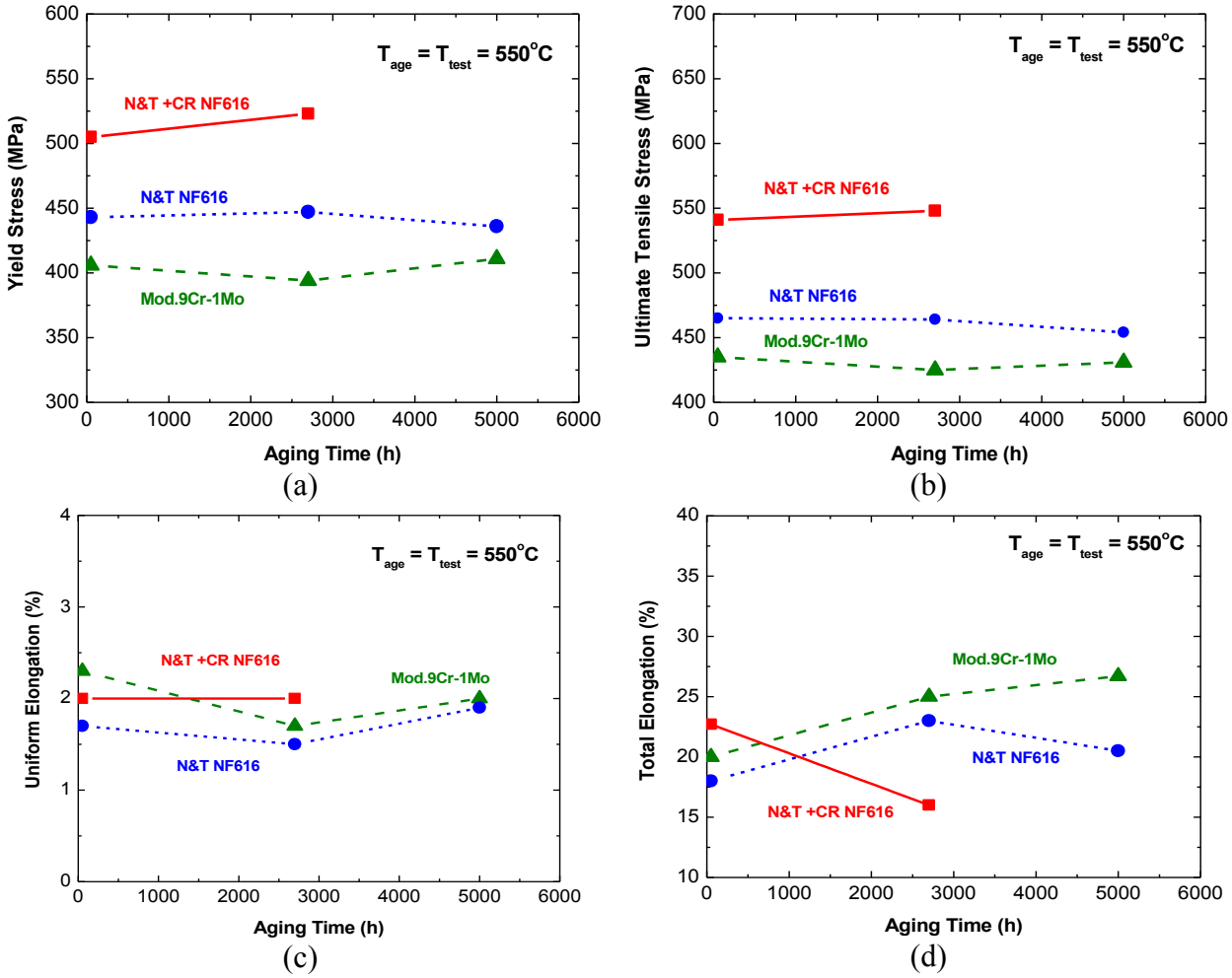


Figure 17. Effect of thermal aging on tensile properties of mod.9Cr-1Mo and NF616 at 550°C.

Table 3. Effects of thermal aging on tensile properties and hardness.

| Alloy | Cond. | Test T (°C) | Strain Rate ($s^{-1}$) | YS (MPa) | UTS (MPa) | UE (%) | TE (%) | HV |
|---|---|---|---|---|---|---|---|---|
| G91 | AR | 20 | 0.001 | 595 | 729 | 8.5 | 18 | 251 |
| G91 | AR | 550 | 0.001 | 406 | 435 | 2.3 | 20 | - |
| G91 | 550°C/2700h Na | 550 | 0.001 | 394 | 425 | 1.7 | 25 | - |
| G91 | 550°C/5000h | 550 | 0.001 | 411 | 431 | 2 | 26.7 | 248 |
| G91 | AR | 600 | 0.001 | 375 | 386 | 1.3 | 28 | - |
| G91 | 600°C/7500h | 600 | 0.001 | 337 | 348 | 1.3 | 32 | - |
| G91 | AR | 650 | 0.001 | 237 | 269 | 2.6 | 46.5 | - |
| G91 | 650°C/1344h | 650 | 0.001 | 252 | 259 | 1.1 | 41 | 237 |
| G91 | 650°C/5000h | 650 | 0.001 | 233 | 245 | 1.2 | 42.5 | 232 |
| G91 | 650°C/10650h | 650 | 0.001 | 248 | 255 | 1.2 | 30 | - |
| H1 NF616 | AR | 20 | 0.001 | 638 | 761 | 7.1 | 16 | 261 |
| H1 NF616 | AR | 550 | 0.001 | 443 | 465 | 1.7 | 18 | - |
| H1 NF616 | 550°C/2700h Na | 550 | 0.001 | 447 | 464 | 1.5 | 23 | - |
| H1 NF616 | 550°C/5000h | 550 | 0.001 | 436 | 454 | 1.9 | 20.5 | 265 |
| H1 NF616 | AR | 600 | 0.001 | 386 | 417 | 1.5 | 27 | - |
| H1 NF616 | 600°C/7500h | 600 | 0.001 | 391 | 400 | 1.2 | 20 | - |
| H1 NF616 | AR | 650 | 0.001 | 295 | 315 | 1.7 | 28 | - |
| H1 NF616 | 650°C/1344h | 650 | 0.001 | 257 | 281 | 1.3 | 26.3 | 245 |
| H1 NF616 | 650°C/5000h | 650 | 0.001 | 280 | 283 | 1.4 | 30.5 | 242 |
| H1 NF616 | 650°C/10650h | 650 | 0.001 | 254 | 268 | 1.5 | 31.5 | - |
| H2 NF616 | AR | 20 | 0.001 | | | | | |
| H2 NF616 | AR | 550 | 0.001 | 505 | 541 | 2 | 22.7 | |
| H2 NF616 | 550°C/2700h Na | 550 | 0.001 | 523 | 548 | 2 | 16 | |
| H2 NF616 | AR | 600 | 0.001 | 398 | 421 | 2 | 32.5 | |
| H2 NF616 | AR | 650 | 0.001 | 274 | 294 | 2 | 52 | |
| H2 NF616 | 650°C/1200h | 650 | 0.001 | 145 | 182 | 5 | 55 | |

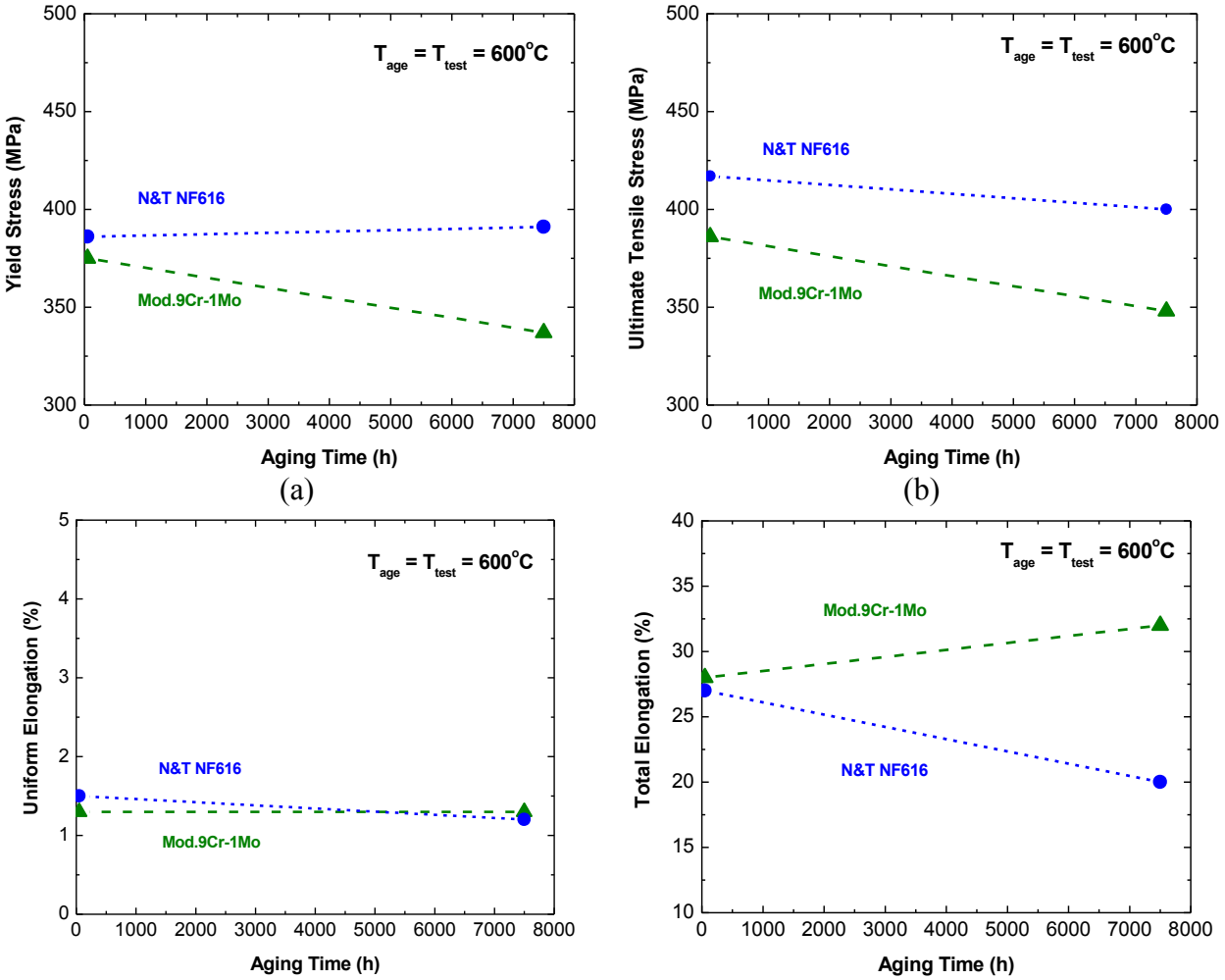


Figure 18. Effect of thermal aging on tensile properties of mod.9Cr-1Mo and NF616 at 600°C.

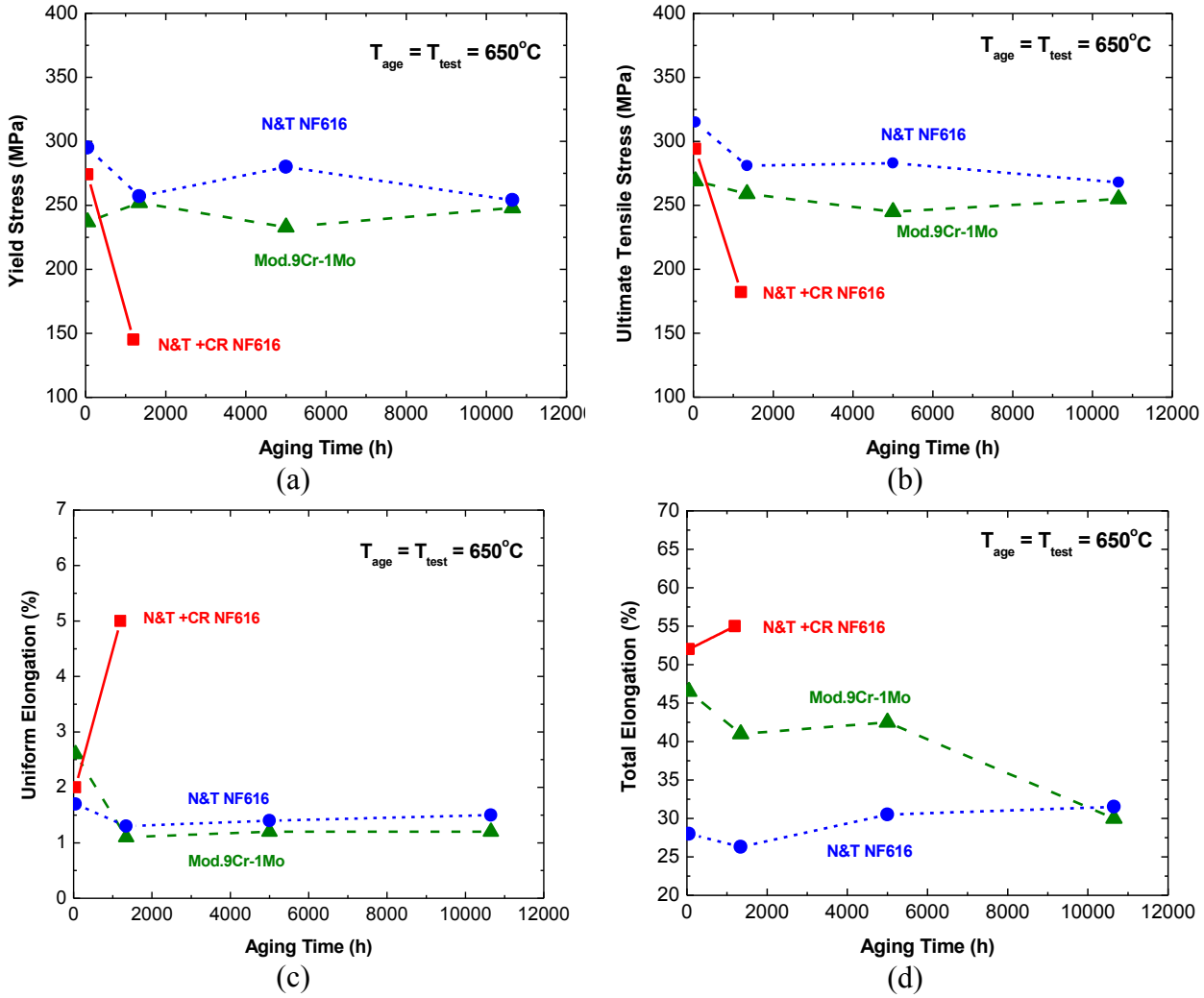


Figure 19. Effect of thermal aging on tensile properties of mod.9Cr-1Mo and NF616 at 650°C.

### *4.3 In-situ* Tensile Testing with Simultaneous Synchrotron XRD Measurements

Deformation process in normalized and tempered mod.9Cr-1Mo steel has been investigated using high-energy synchrotron x-ray diffraction during *in situ* tensile loading at 20 and 550°C. The response of different lattice planes to the applied tensile load can be monitored measured in real time. Figure 18 shows the macroscopic stress-strain curves constructed from the load and displacement data for G91 steel tested at 20 and 550°C, respectively. The alloy shows significant strain hardening at 20°C, while very limited hardening and strong localized deformation at 550°C. This dramatically different deformation behavior provided an ideal case for understanding strain hardening and softening effects and localized deformation using the in-situ XRD technique.

Figure 19(a) and (b) shows the response of the lattice strain in the axial (loading) direction to the applied stress up to the maximum load at 20 and 550°C, respectively, for the diffraction

peaks (110), (200), (211), and (310) of the body-centered cubic (bcc) matrix of the G91 steel tested. The microscopic stress-strain response at 550°C is significantly different from the 20°C deformation behavior. Lattice strain determined by a relative change in lattice spacing in a microscopic volume can be used as an internal strain gauge to probe the mechanical response of the material during loading and unloading.

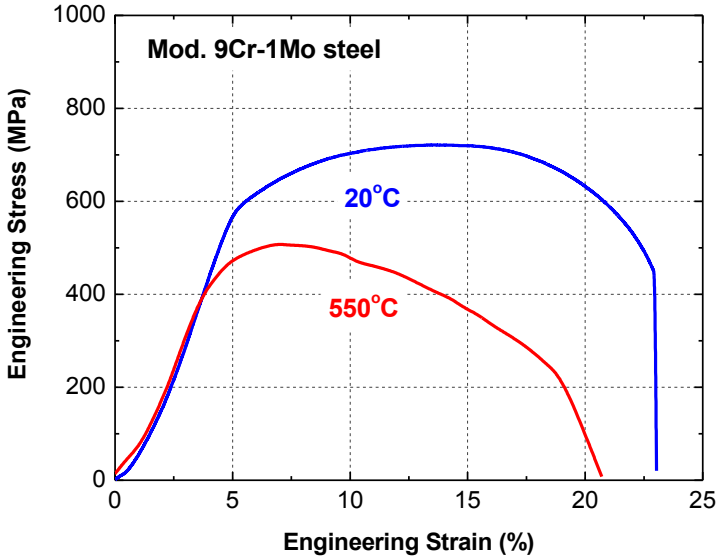


Figure 20. Engineering stress-strain curves for mod.9Cr-1Mo *in situ* tensile tested at 20 and 550°C.

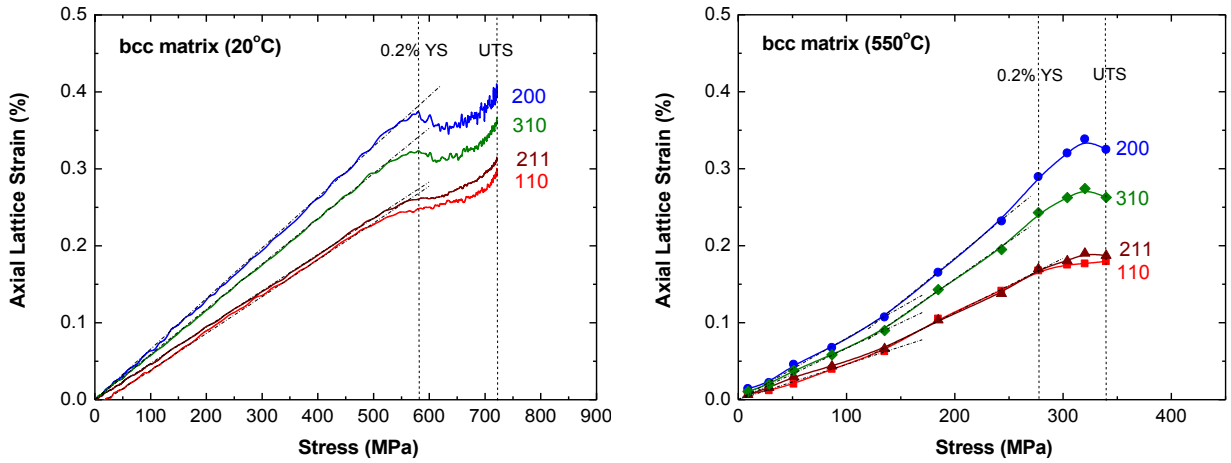


Figure 21. The evolution of lattice strain in axial direction as a function of the applied stress for mod.9Cr-1Mo steel, *in situ* tensile tested at (a) 20°C and (b) 550°C.

Figure 20(a) and (b) shows the relative change of the full width at half maximum (FWHM), i.e. (FWHM(ε)-FWHM(0))/FWHM(0), as a function of the applied stress for the 110, 200, 211, and 311 Bragg peaks for the mod.9Cr-1Mo in situ tensile tested at 20 and 550°C. Detailed analysis of x-ray diffraction line profiles can provide dislocation density changes during annealing.

Figure 21 shows the lattice strain response to the applied stress of the $M_{23}C_6$ phase in the axial and radial directions, respectively, up to the maximum load for the (422) diffraction peak of $M_{23}C_6$ ($Cr_{23}C_6$) along with the (110) diffraction peak of the bcc matrix of mod.9Cr-1Mo steel. The lattice strain evolution is divided into three stages, i.e. elasticity, micro-plasticity and macro-plasticity.

In the elastic regime, both the bcc matrix and the carbide deform in a linear fashion with similar slopes. Deviations from this initial linearity occur at 135 MPa (micro plasticity), and the slopes for both the bcc matrix and the carbide phase in the axial direction were reduced. The carbide phase showed a much lower slope than the bcc matrix, which indicates that the carbide phase carries more load than the bcc matrix. The second inflection occurs at the 0.2% yield point (277 MPa) in bcc matrix (macro plasticity), while the linear function of the carbide phase remains the same.

In the macro-plasticity regime, the bcc matrix showed a continuous increase in slope up to UTS, while the carbide phase showed an inflection at 304 MPa and elastic contraction at 320 MPa. The maximum ratio of the axial lattice strain of the carbide phase and the bcc matrix is 1.67 (at the stress level of 320 MPa), an indicator of the level of loading shedding from matrix to the second phase. The lattice strain response in the radial direction is less informative than that in the axial direction. This type of *in situ* experiments has shown a remarkable value in the development of the microstructure-property model.

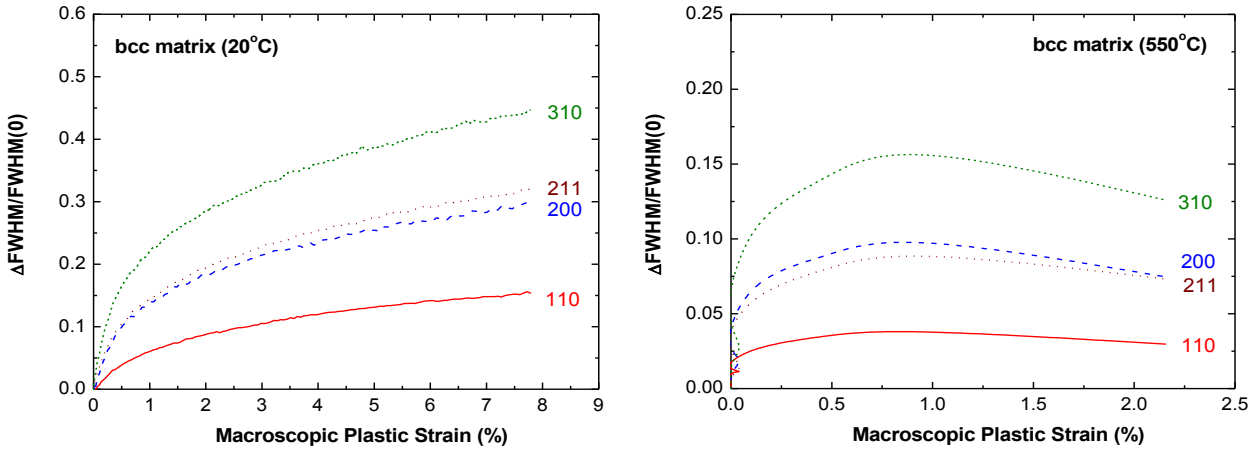


(a) (b)

Figure 22. Peak broadening as a function of plastic strain for mod.9Cr-1Mo steel *in situ* tensile tested at (a) 20°C and (b) 550°C.

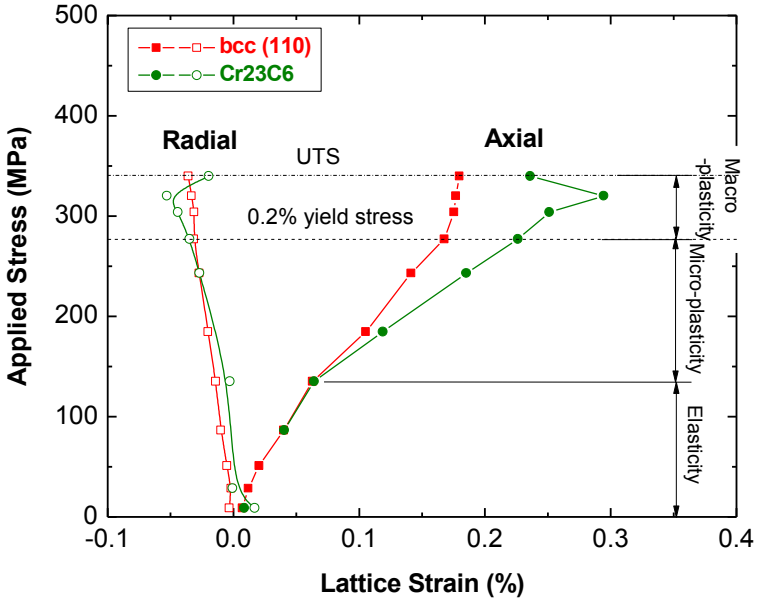


Figure 23. Load partitioning between the bcc matrix and $Cr_{23}C_6$ phase in mod.9Cr-1Mo steel *in situ* tensile tested at 550°C.

# 5 Summary

This report provides an update on the evaluation of thermal-aging induced degradation of tensile properties of advanced ferritic-martensitic steels. Five alloys are examined, mod.9Cr-1Mo, NF616 with two different thermal-mechanical treatments, and solution-annealed HT-UPS and hot-rolled HT-UPS. The report summarizes the tensile testing results of thermally-aged mod.9Cr-1Mo, NF616 H1 and NF616 H2 ferritic-martensitic steels. NF616 H1 and NF616 H2 experienced different thermal-mechanical treatments before thermal aging experiments. NF616 H1 was normalized and tempered, and NF616 H2 was normalized and tempered and cold-rolled. By examining these two heats, we can assess the effects of thermal-mechanical treatments on materials' microstructure and associated mechanical properties during long-term aging at elevated temperatures.

Thermal aging experiments at different temperatures and periods of time have been completed: 550°C for up to 5000 h, 600°C for up to 7500 h, and 650°C for more than 10,000 h. Tensile properties were measured on thermally aged specimens and aging effect on tensile behavior was assessed. Effects of thermal aging on deformation and failure mechanisms were investigated by using *in-situ* straining technique with simultaneous synchrotron XRD measurements.

# References

Busby, J., T. S. Byun, R. Klueh, P. Maziasz, and J. Vitek, K. Natesan, M. Li, R. Wright, S. Maloy, M. Toloczko, A. Motta, B.D. Wirth, G. R. Odette, T. Allen, "Candidate Developmental Alloys for Improved Structural Materials for Advanced Fast Reactors," ORNL/GNEP/LTR-2008-023, March 2008.

Klueh, R. L. and D. R. Harries, High-Chromium Ferritic/martensitic and Martensitic Steels for Nuclear Applications, ASTM, West Conshohoken, (2001).


**Nuclear Engineering Division**
Argonne National Laboratory
9700 South Case Avenue
Argonne, IL 60439

www.anl.gov